Laser Crosslink Atmospheric Sounder to Investigate the Effects of Deep Convection on Ozone

Cadence Payne, Angela Crews, Paul Serra, Kerri Cahoy, Alexa Aguilar, Peter Grenfell, Haeyoung Choi
Massachusetts Institute of Technology, Department of Aeronautics and Astronautics, Space Telecommunications, Astronomy, and Radiation Laboratory
77 Mass. Ave., 37-315, Cambridge, MA 02139; (617) 452-3840
cbpayne@mit.edu

John Conklin
University of Florida, Precision Space Systems Laboratory
Gainesville, FL Gainesville, FL 32611

ABSTRACT

Deep convection at mid-latitudes can directly inject water vapor into the upper troposphere/lower stratosphere (UTLS). Increased water vapor creates a photochemical environment that can activate inorganic chlorine (HCl) which then catalytically destroys ozone, increasing health and environment risk [1]. The Laser Crosslink Atmospheric Sounder (LCAS) is a prototype toward a low-Earth-orbiting (LEO) constellation to concurrently measure both UTLS water vapor and temperature at high vertical resolution, improving temporal and spatial coverage. The two-part approach uses both beam pointing and intensity. First, precision pointing measures atmospheric refraction and can be used to obtain temperature profiles [2]. Second, intensity on the continuum and near absorption features of the spectrum can measure water vapor concentration.

This work presents demonstration using near-infrared laser crosslinks wavelengths in ITU-S (1460 nm to 1530 nm) and ITU-C (1530 nm to 1565 nm) bands for measurement of water vapor, where commercial components already exist for applications like coarse wavelength division multiplexing (CWDM) over terrestrial optical fiber. We use MODTRAN to assess the measurability of varying concentrations of water vapor in the UTLS in these bands. We find that 1550 nm is a suitable continuum reference wavelength, and that 1504 and 1509 nm have detectable changes in transmissivity with increases in water vapor.

INTRODUCTION

The miniaturization of commercially available subsystems and components is improving the scientific capability of CubeSats for Earth Observation as well as improving the bandwidth of CubeSat communication systems. This paper presents a concept for using technologies currently in development for a laser crosslink communications system as a sensor of atmospheric temperature, pressure, and composition.

Project Motivation

Thunderstorms and convective storms transfer water vapor into the Earth's UTLS. Anderson *et al.* has measured that excess water vapor content in the UTLS results in a photochemical environment activating inorganic Chlorine (HC1), which can lead to decreased ozone and increased risk of UV exposure [1].

Water vapor is a dominant contributor to the dynamic nature of the Earth's climate and weather systems. Stratospheric H2O has been known to sporadically fluctuate, with links to deep tropical convection (e.g., thunderstorms) [1]. The decrease in O3 is related to both an increase in water vapor and temperature. To assess these relationships, it is necessary to measure water vapor and temperature concurrently. This can be done *in situ* over limited regions using aircraft. Satellite instruments can also make these measurements, but not yet concurrently and at high vertical resolution. For example, GPS Radio Occultation (GPS RO) can measure temperature profiles with high vertical

resolution, but not water vapor concentrations, since the GPS RO measurements are restricted to the GPS radio wavelengths.

Laser crosslinks have a similar tangential sounding of the atmosphere geometry to GPS RO (as shown in Figure 3). If the wavelengths for a crosslink experiment are chosen such that they sample water vapor continuum and absorption features, we can measure concentration [3]. This can be done for any species of interest. If we track beam angle of arrival (mispointing) we can measure refraction and measure temperature (see Sterr et al. 2016 [4], Figure 5).

Difference between LCAS and prior studies

The concept of laser occultation for atmospheric composition has been well-studied as part of a previous ESA proposal called "ACCURATE: climate benchmark profiling of greenhouse gases and thermodynamic variables and wind from space," [3, 6]. There are several key differences between LCAS and the ACCURATE proposal. (i) LCAS is a small satellite demonstration targeting just water vapor, where ACCURATE considered several molecules. (ii) The ACCURATE mission approach required active microwave crosslinks as well as active optical crosslinks. (iii) ACCURATE optical links provided intensity-only differential-paired measurements that yielded composition, and the high resolution temperature profiles came from the microwave links; LCAS will provide both, from the laser crosslink by tracking bending angle. (iv) The novel contribution from LCAS is the inclusion of precision ranging and pointing to directly recover bending angle information from the laser crosslink, which allows the laser link to be used for high vertical resolution temperature-pressure profile retrieval. (v) LCAS can demonstrate this capability leveraging low-cost, compact, commercial optical communications components and newly developed nanosatellite technologies [6].

To summarize, with LCAS we build upon the significant recent work done with ACCURATE and in nanosatellite optical communications to propose an initial demonstration with the novel approach of a laser occultation system using precision optical time transfer for ranging, precision internally-calibrated fine pointing and a new star-tracker-based estimator for accurate attitude determination, and leveraging commercially available optical communications components in the ITU bands to keep the system low-cost and compact, suitable for a CubeSat or small satellite [7 , 8].

Mission Objectives

The science performance goals for LCAS are motivated by characterization of convectively injected water vapor in the upper troposphere and lower stratosphere (UTLS) region, and its effect on ozone. LCAS will obtain both composition and temperature with high vertical resolution profiles by directly measuring the bending angles and ranges between the satellites. The LCAS demonstration goal, focusing on H_2O in the Upper Troposphere and Lower Stratosphere region, is to achieve better than 3% volume mixing ratio profile measurements with better than 1 K accuracy and 0.5 K precision and less than 250 m vertical resolution.

Scientific Relevance

One example of a scientific contribution that the LCAS system would make is the investigation of how much water vapor is injected into the UTLS region by convective storm systems. Deep convection in the tropics are important in regulating climate, to study mass transport to the upper atmosphere and how it moves towards the poles. Climate models need input on how much water vapor moves up and to the poles (which are deserts) due to storm convection, and it is difficult to measure water vapor within the storms themselves. The convectively injected water vapor plus a decrease in temperature (both must be measured) in the UTLS contributes to the depletion of ozone at mid-latitudes, possibly fractional reductions of as much as 17%, which could have both climate as well as human (UV radiation) impacts [1]. It is important to understand how this ozone reduction process works currently, and to compare it to future years when there may be increases in the number of storms. The laser occultation system would need to be capable of measuring increases in water vapor in the UTLS (e.g., 12 km to 20 km altitude) from 4.5 ppmv to 10 ppmv (the modeled increase resulting in the 17% fractional reduction of ozone), but increases as high as 18 ppmv were measured *in situ*. The laser occultation system would need to be capable of measuring temperature profiles with an accuracy, based on in situ measurements from NASA SEAC[4]RS used in the analysis (Figure 4 in Anderson 2017 [1]), of < 1 K and vertical resolution of < 0.5 km. There are several other examples of how measurements of atmospheric water vapor and gases in the UTLS would better inform our understanding of weather, cloud formation, and climate as well, such as measurements of UT super-saturations

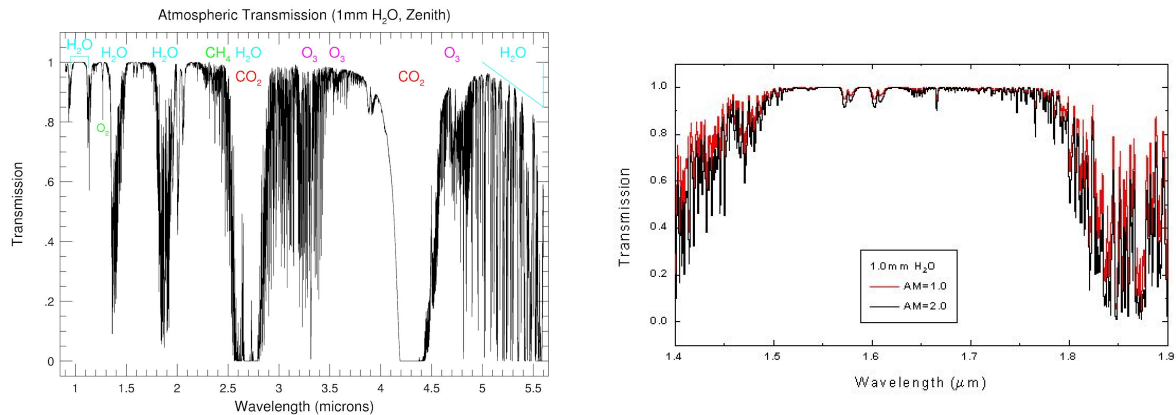of water vapor, stratospheric desaturation, and atmospheric rivers.

Figure 1 Atmospheric transmission spectrum of air. (a) Near infrared transmission spectrum, showing H2O, CO2, O3, and CH4 [10]. (b) Comparison of transmission spectra at air mass 1 and 2 (zenith and ~60 degrees off zenith) with 1 mm precipitable water vapor. Even from the ground, there are discernable differences observed in this wavelength region [11]. See the MODTRAN analysis the Approach section for more detail.

Improvement of the Science Measurement

The data needed to study the convective injection of water vapor into the UTLS and its effect on relative ozone fraction are co-located and concurrent measurements of both water vapor concentration as a result of convective injection from storms, and temperature as a function of height, augmented by measurements of ozone and trace species. The information needed for this analysis at the desired horizontal and vertical resolution can currently only be obtained from multiple satellite and in-situ measurements. In Anderson 2017, these included convective weather activity using radar systems such as NEXRAD, water vapor estimates inferred from HDO to H2O ratios from the atmospheric chemistry experiment Fourier Transform Spectrometer (ACE-FTS), trace species from the Aura Microwave Limb Sounder whose microwave radiometers also provide water vapor and temperature profiles, but with larger horizontal and vertical resolution, on the order of tens of km to a few km, and in situ ozone data from the NASA Studies of Emissions and Atmospheric Composition, Clouds, and Climate Coupling by Regional Surveys (SEAC⁴RS) mission [1, 9].

Laser occultation can make global, persistent measurements of temperature and atmospheric species concentrations in the UTLS, and can improve on the vertical resolution possible with GPSRO. Using paired, proximal wavelengths that concurrently

sound both near or within an absorption feature of the species of interest as well as along the continuum permits retrieval of concentration, as the intensity fluctuations caused by atmospheric turbulence along an identical path can be differenced such that their net effect on the measurement is negligible [3].

While in the near-IR there are many absorption features to choose from with detectable attenuations over the crosslink path, to take advantage of the commercially developed components for optical communications (see Figure 1), for a low-cost, compact crosslink demonstration instrument, it is a logical choice to target water vapor. It is true that optical links are limited by the presence of clouds, which means such measurements at times can be infeasible in the lower troposphere, so sounding in the UTLS region is appropriate for this measurement approach. We can validate the laser occultation temperature retrievals with an onboard GPSRO receiver, and validate the higher resolution temperature as well as water vapor measurement accuracy with airborne *in situ* measurements. Concerns about measurement effects such as defocusing, foreign species absorption, aerosol extinction, Rayleigh scattering, clouds, turbulence, background and scattered light, and thermal effects are discussed extensively in Schweitzer et al. 2011 [3]; to summarize: effects are negligible for carefully designed systems with small apertures, and for targeted measurements in the UTLS.
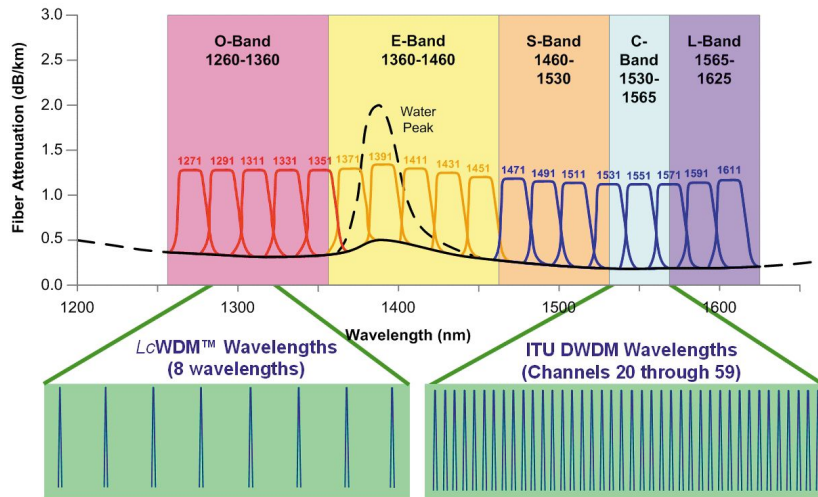
Figure 2. A demonstration mission can leverage hardware within the ITU optical communications bands used for wavelength division multiplexing. Note that this figure references the attenuation in fiber, not in atmosphere [12].
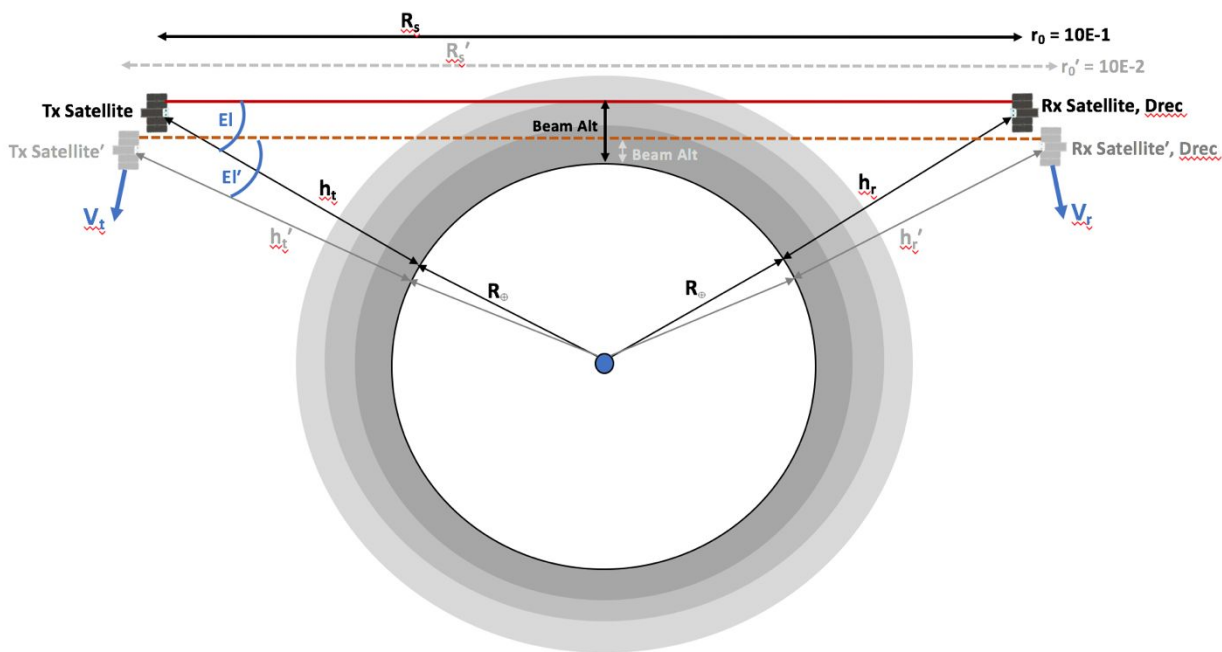

Figure 3. Laser Occultation experiment geometry [13]. Demonstrating the transmitting (tx) and receiving (rx) s/c with optical links traversing the Earth's atmospheric limb. For each spacecraft, two instances in time are shown. Rs and Rs' are ranges between rx and tx s/c during initial acquisition and a later time as satellites are setting in their orbits, r_0 and r_0' are ranges between tx and rx s/c at initial acquisition and a later time, beam altitudes are the tangent point - the distance between traversing optical beams and Earth's surface, $R_\oplus$ is radius of Earth, h_r and h_r' are heights of satellites above the surface of the Earth at initial acquisition and a later time, El and El' are elevation angles for tangential heights (h_r and h_r') and the transmitted beam between rx and tx, and V_r and V_t are velocities of rx and tx s/c respectively.
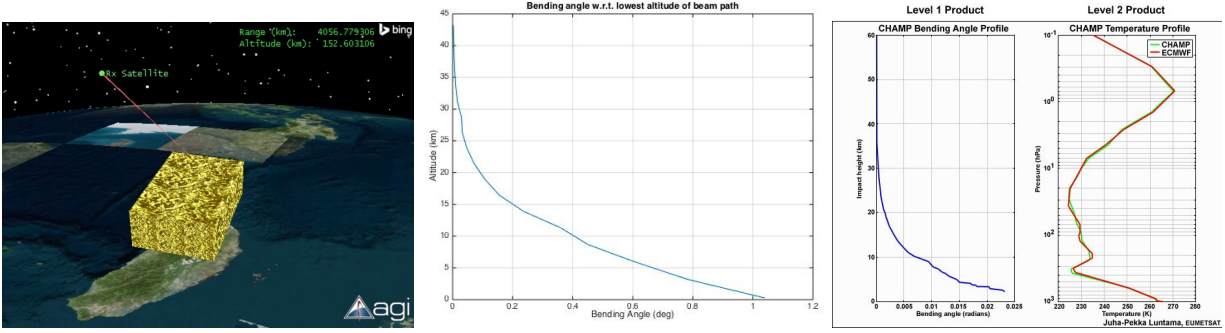
Figure 4 (a) Visualization of a crosslink between two LEO 6U CubeSats using AGI STK. (b) Bending angle at 1550 nm between two occulting LEO satellites with 600 km orbit altitude crosslinks through 'dry air' atmosphere using NIST refractive index of air calculator shows measurable bending on the order of half a degree at 10 km altitude; simulation courtesy Hyosang Yoon (MIT). (c) CHAMP GPSRO [16] bending angle and temperature profile plot for comparison, at 10 km 0.01 radians is also on the order of 0.5 degrees or 1800 arcseconds (bending for near infrared lasers is not exactly the same as at GPS wavelengths, but is within 6%, so this is still a relevant comparison) [3].

APPROACH

The novel technology is a laser occultation crosslink instrument that includes precision ranging and optical time transfer, as well as precision pointing.

Concept of Operations

This work considers a technology demonstration of the laser occultation concept using nanosatellites, such as CubeSats. While an operational system may require a larger platform to accommodate a laser transceiver system capable of supporting more wavelengths with improved stability and perhaps tunability, as well as a more responsive attitude determination and control system, demonstration with a nanosatellite crosslink would provide cost-effective technology maturation and risk reduction. Figure 4a shows a notional CubeSat implementation scheme for a demonstration. There are many orbital configurations that would support a occultation crosslink. This example scenario has two CubeSats that are in 500 km counter-rotating orbits (one at 80 deg inclination and 0 deg right ascension of the ascending node (RAAN), the other at 100 deg inclination and 180 deg RAAN) would obtain 31 along-track occultation measurements of UTLS water vapor and temperature with high vertical resolution over one day. Any LEO orbit above a ~500 km altitude will suffice for this demonstration. Differential drag maneuvers, utilizing attitude information from the ADCS, can maintain range control after the simultaneous deployment of both CubeSats.

LCAS has similarities and differences with GPS radio occultation. GPSRO depends on the GPS constellation of satellites in addition to LEO satellites having specially modified GPS receivers capable of rapid dual-band measurements and also high gain dual-band antennas. The L-band frequencies of GPS satellites do not allow the same approach to obtaining composition as proposed for LCAS, as they do not concurrently fall on a water vapor absorption feature and the continuum. LCAS would send wavelength paired signals (one on a still-detectable absorption feature, and one on the continuum) and take the difference between the two to capture composition information, as detailed in Schweitzer et al. 2011 [3].

Figure 3 shows the geometry of a laser occultation experiment. The Laser Crosslink Atmospheric Sounder (LCAS) instrument would have precision timing [19, 22, 23] and pointing capability, in addition to wavelength-stabilized and calibrated, paired, full-duplex crosslink beams, to concurrently recover both composition and temperature with high accuracy and high vertical resolution.

The Fresnel zone for a near infrared laser link is ~3 m [14], and the proposed crosslink beamwidth is 120 urad (~24 arcseconds). Previous demonstrations and a preliminary link analysis show that transmit power on the order of ~1 W will be sufficient to maintain the link for sounding the UTLS, which is confirmed by the authors' preliminary link budget analysis as well as that detailed in Kirchengast and Schweitzer, 2011 [15].
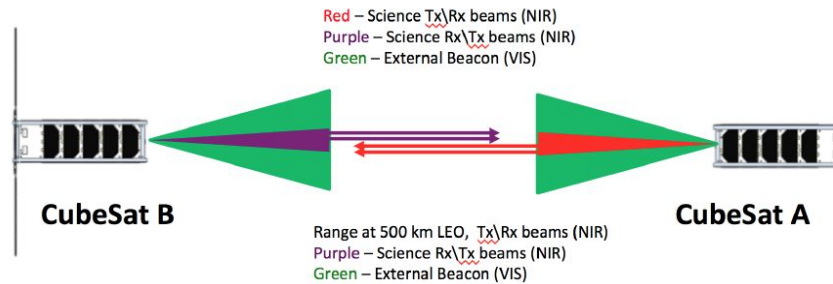
Figure 5. High-level concept demonstrating a laser crosslink between two LEO CubeSats. The green beam is the wider laser beacon used for spacecraft pointing. The purple and red beams are the narrow science beams. Each color represents a differential pair of wavelengths, one at an absorption feature and one at the continuum.

Differences between LCAS and earlier efforts

In the ACCURATE proposal [6], custom microwave crosslinks are needed in addition to the laser links in order for the mission to obtain temperature profiles with high vertical resolution. This is similar to GPS Radio Occultation, but instead of operating at GPS L-band frequencies, operating at select microwave frequencies best suited for either sensing or avoiding atmospheric species such as water vapor [6]. The first mission concept to suggest moving beyond GPS for water-vapor sensitive microwave crosslinks was the Active Temperature, Ozone and Moisture Microwave Spectrometer (ATOMMS) mission [18]. The laser occultation approach in ACCURATE focused on targeting fundamental absorption features, with the laser technology outside of the range where low-cost optical communications components are readily available [12]. We propose with LCAS to take advantage of commercial components for a technology demonstration first, and then scale up. Customization and frequency licensing are also part of the challenge with having an active microwave crosslink sounding other than GPSRO.

For GPSRO, in addition to the having orbit information for the transmitting GPS satellite and the receiving LEO satellite, reference measurements are needed, such as from an additional, non-occulting, GPS satellite to the LEO, and reference measurements from the non-occulting GPS satellite to ground [17]. This is because with GPSRO we must calculate phase residuals; we must first determine what the received signal would have been if it had been traveling along line-of-sight (LOS) through 'empty space' instead of traveling through the changing refractivity of the atmosphere. So, the geometry of the entire system as a function of time

needs to be estimated accurately enough to remove the predicted LOS received signal from the measurement, and to keep only the 'phase residuals' which capture the information about density (and thus temperature and pressure) with height.

After the demonstration LCAS laser occultation experiment with fixed wavelengths, it may be that using a more sophisticated instrument with pulsed output from tunable, calibrated wavelength division multiplexing laser transmitters would be reasonable. The Grace Follow On Mission uses a Laser Ranging Interferometer at 1064 nm but the spacecraft separation is only on the order of hundreds of km and not far enough to support an occultation crosslink [26]. The LCAS approach takes an incremental but important technology development step toward more targeted and sophisticated instruments.

Precision Ranging and Optical Time Transfer

Precision ranging is required in order to obtain a precise bending angle. The solution for LCAS is to use the time of flight (TOF) of short optical pulses at wavelengths around 1550 nm. As the optical peak-power of lasers available on CubeSats is limited, a dual one-way ranging scheme has been selected. This scheme also allows optical communication encoded with Pulse-Position Modulation (PPM), and is identical to the solution developed for the CubeSat Laser Infrared CrosslinK (CLICK) payload [22, 23, 24].

The one-way ranging scheme is based on two clocks, one in each satellite. The CubeSat A sends a pulse at a known time against its own clock. The pulse travels to CubeSat B, which records the time of arrival against its own clock. CubeSat B also emits a pulse referenced on its clocks, which is received and timed

by CubeSat A. With those four times, both the range between the satellites and the clocks' discrepancies can be calculated. The timestamps recorded by both satellites can be exchanged on the optical links.

The hardware required to support this scheme is derived from the CLICK mission [22, 23, 24]. On the emitting CubeSat, a seed laser based on amplitude/frequency modulation, similar to the one described by Kingsbury in [25] is used to obtain optical pulses at the desired wavelengths in the 1550 nm band. Those pulses are then amplified by an Erbium-Doped Fiber Amplifier (EDFA). On the receiving CubeSat, an avalanche photodetector converts the optical pulses into a current, and an amplificator chain with programmable gain adapts the signal for two possible converters. The receiver is equipped with both a fast Analog-to-Digital Converter (ADC) and a Time-to-Digital Converter (TDC). The ADC supports up to 500 million samples by second, and is used with a Matched-Filter (MF) DSP algorithm. To complement the TDC, the ADC-MF receiver should be capable of recovering data when the signal-to-noise ratio is low and no clear edge is available on the received pulses. The TDC-based receiver requires a clean pulse edge. This receiver directly provides timestamps, which greatly simplifies post-processing, and is more accurate for ranging when noise is low. A pulse timing accuracy of 50 ps can be achieved with this receiver. The clock used in both CubeSats is a compact, low power cesium oscillator, such as the Microsemi Chip-Scale Atomic Clock (CSAC). The clock is used as a reference for the time-of-flight, and also to keep time if the two one-way ranging operations cannot occur simultaneously.

A prototype of the transceiver, constructed in the Precision Space Systems Lab at the University of Florida, is shown in Figure 8 [19]. This setup currently includes a Smartfusion2 FPGA, a CSAC, and a custom interface board. It is used to validate the timing accuracy of the modulator. A complete transceiver including both converters and compatible with the CubeSat form-factor is currently in joint development by University of Florida and MIT for CLICK.

Pointing, Acquisition, and Tracking

In order to establish and maintain the laser crosslink for the duration of the experiments, a three-stage pointing, acquisition, and tracking (PAT) system is implemented. The initial analysis for the CLICK version of this system is documented in Long [23].

The first stage is acquisition. In nominal operations, this consists of the spacecraft receiving GPS ephemeris data from its partner spacecraft and inertially pointing to the resultant relative pointing direction. The CLICK payload beacon optics are designed for stare-stare acquisition, which means that the beacon divergence angle is such that given expected GPS, ADCS, and optomechanical errors, each spacecraft will be within the 2700 arcsec (0.75°) FWHM cone of the other spacecraft's beacon at the start of a crosslink event, before the signal begins to enter the denser regions of the atmosphere (see Table A.5). The ionosphere does not significantly affect near infrared wavelengths.

The next stage in the sequence is coarse tracking using the Coarse Pointing System (CPS). The CPS closes the loop on inertial spacecraft pointing to enable coarse tracking within the limitations of the hardware and data communications systems. The CPS data sources consist of on-board GPS-based position data, attitude data, the partner satellite's GPS data, and beacon camera image data. Note that GPS receiver data for orbit determination is common for LEO and less complex than a GPSRO experiment. A real-time relative pointing estimator (the satellite tracking Kalman filter [8]) is implemented that synthesizes this data and enables pointing corrections to be sent to the ADCS.

Simulations of the CPS have been created and the results were used to design the final stage of the PAT system: the Fine Pointing System (FPS) (see Table A.6). The elements of fine pointing control consist of a MEMS fast steering mirror (FSM), which actuates the incoming and outgoing beams, and a quadrant photodiode detector (quadcell), which detects the beacon signal and provides feedback to the FSM. In the LCAS optical design, the FSM used is referred to as FSM 1. This system has been characterized by hardware-in the loop testing and Zemax modeling and is expected to satisfy the pointing requirement (see Table A.7). Updates to the CLICK design for the LCAS requirements is an area of future work.
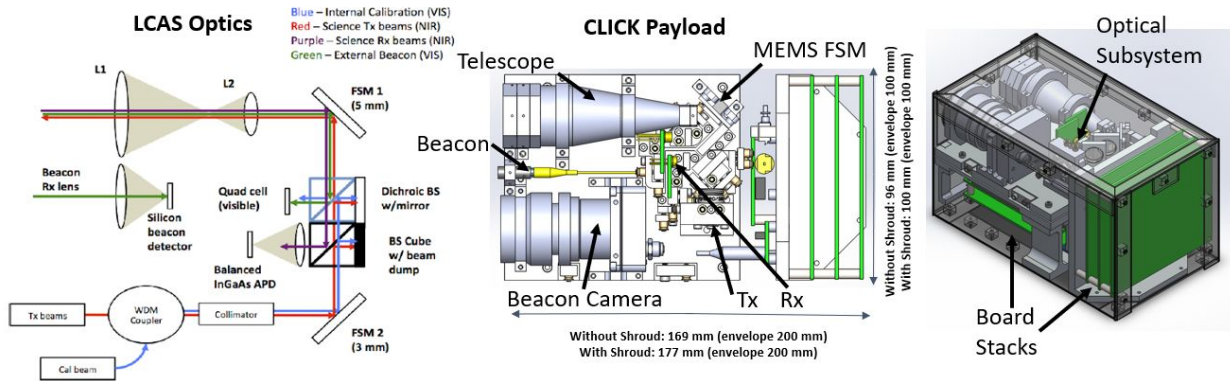
Figure 7. (a) Initial optical diagram for the LCAS transceiver. (b) MIT CAD rendering of a CubeSat form-factor crosslink optical terminal for the CLICK mission.
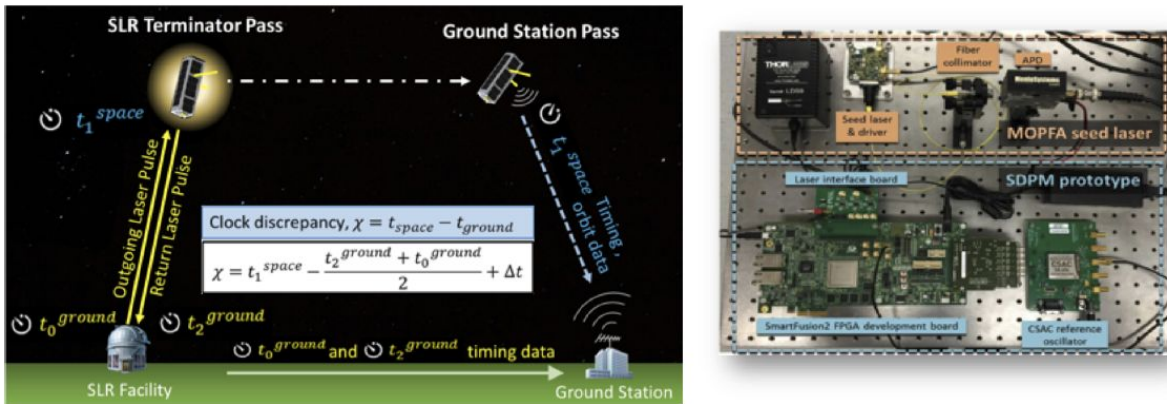

Figure 8. Precision ranging is possible using the optical time transfer technology developed by the University of Florida for the CHOMPTT (CubeSat Handling Of Multisystem Precision Time Transfer). Applying CHOMPTT technology for crosslinks is demonstrated with the MOCT (Miniature Optical Communications Transceiver) prototype [19]. Precision ranging is needed for temperature profile retrieval, as LCAS will need precise orbit determination for comparison of the "vacuum" propagation to atmospheric propagation. [17]
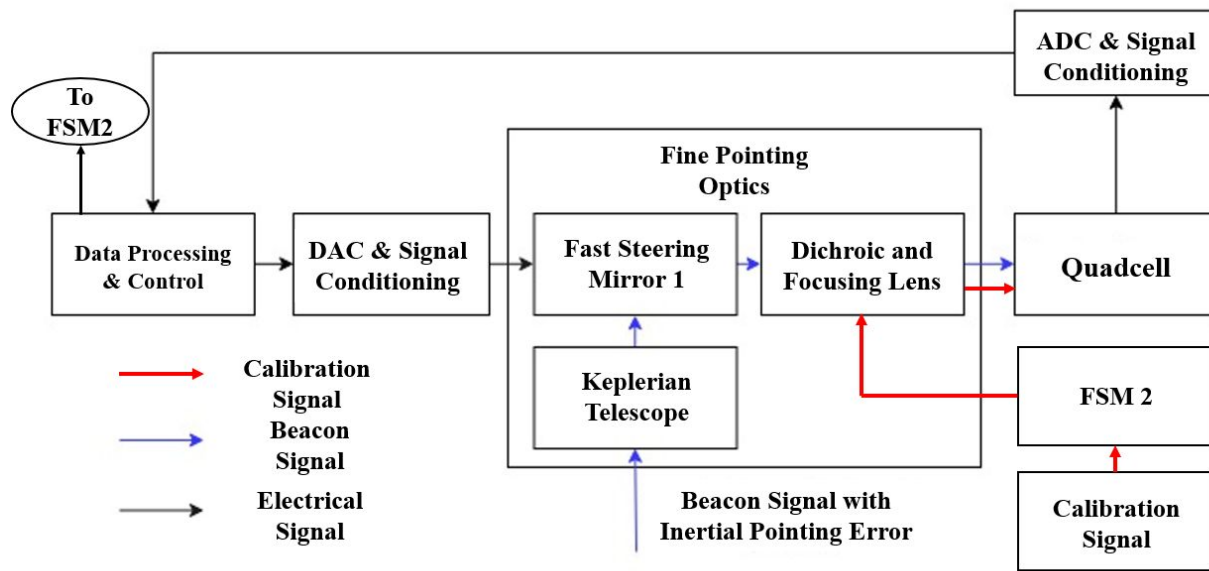
Figure 9: LCAS Fine Pointing System Diagram. Mission functionality is assessed with spacecraft-induced disturbance mitigation for the APD sensor using a quadcell and FSM 1, and measurement of bending angle using a quadcell.

Measuring Bending Angle Approach

The bending angle is normally obtained in a GPS radio occultation experiment by measuring the L-band phase residuals due to the longer refracted path through the atmosphere as its density increases with decreasing altitude, compared with the line-of-sight path through "empty" space. For LCAS, we will instead directly measure the bending angle along the crosslink path in order to provide an occultation retrieval of a temperature profile using the laser occultation signal.

LCAS can demonstrate this capability leveraging low-cost, compact, commercial optical communications components and newly developed nanosatellite technologies. LCAS will augment orbit determination from onboard GPS receivers with precision optical angle of arrival tracking and optical time transfer techniques recently developed at MIT and the University of Florida, and will leverage precision pointing developed for MIT/UF missions Nanosatellite Optical Downlink Experiment (NODE) [27] and CLICK [19, 22, 23].

As shown by Sterr et al., laser beam deflections from atmospheric effects cause measurable pointing error effects at LEO. [4] Geostationary (GEO) to LEO crosslinks have been demonstrated and pointing

errors shown for links down to grazing altitudes of 40 km with documented "LEO Mispointing" of up to 300 μrad (61 arcseconds, 0.01 degrees). [4] . We will measure the laser beam deflection through the atmosphere with an adapted version of CLICK's fine pointing system in order to obtain the bending angle along the crosslink path.

A notional fine pointing system is shown in Figure 9. The system is composed of a First Sensor QP1-6 quadrant photodiode detector (quadcell) which is used to detect the beacon and calibration signals, and a Mirrorcle microelectromechanical system (MEMS) Fast Steering Mirror (FSM), which is used to maintain alignment of the transmit and receive signals. The quadcell receives the beacon and calibration signals via wavelength-division multiplexing as in Miller et al. [21]. The receive angle is calculated by post-processing the spot locations and FSM control data. The data processing algorithm calculates a pointing equivalent angle for the incoming beacon spot by batch least squares estimation.

LCAS would also use APD receivers (commercially available in the near infrared courtesy of terrestrial fiber optic networks) to enable both measuring composition at high vertical resolution as well as bending angle (as described above) and the range

(using technologies similar to the University of Florida MOCT transceiver), from which high vertical resolution temperature profiles could be recovered.

Refractivity can be derived from bending angle using techniques such as the Abel transform [2]. Atmospheric properties such as density, pressure, and temperature can be derived from refractivity using the ideal gas law and the equation of hydrostatic equilibrium [2]. LCAS will use these techniques to derive temperature profiles from the bending angle.

Measuring Water Vapor, MODTRAN Analysis

LCAS will measure water vapor by determining intensity on the continuum and near absorption features. Paired, proximal wavelengths will concurrently sound near an absorption feature of water vapor and along the continuum and measure attenuations over the crosslink path. Identification of absorption features that provide measurable changes in intensity but not complete signal loss is needed. We first consider whether commercially developed components for optical communications are useful for targeting water vapor. We use MODTRAN to simulate a 100 km altitude observer (maximum altitude for this geometry in MODTRAN, but extending through "empty" space to a higher altitude will not impact results) to tangent heights of 10 km, 15 km, and 20 km. Figure 10 shows this geometry for a tangent height of 10 km.
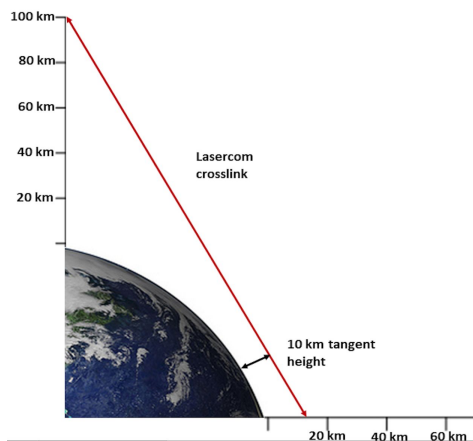

Figure 10. This snapshot of the MODTRAN analysis geometry depicts an observer at 100 km with a tangent height of 10 km to simulate the lasercom crosslink geometry between the CubeSats. Note that a full crosslink occultation path would be twice that simulated by MODTRAN here.

In order to select paired, proximal wavelengths for use with LCAS, we analyze atmospheric transmissivity over 1500 nm to 1600 nm as we use MODTRAN to adjust the scale value of water vapor for a crosslink through the UTLS. We study transmissivity changes at 10 km, 15 km, and 20 km with a scaling factor for water vapor of 1.0, 2.0 and 3.0, as a simple way to capture changes water vapor concentration levels that are doubled and tripled as shown in Anderson's ozone reduction analysis for water vapor increasing from 4.5 to 18 ppmv [1]. We will continue to develop more sophisticated MODTRAN models and retrieval methods, but this approach is used for an initial assessment. We find that water vapor scale factors of 2.0 and 3.0 are nearly identical within the 1500 nm to 1600 nm range (although they are measurable at other wavelengths), and here focus on comparisons below between the 1.0 and 2.0 scaling factors.
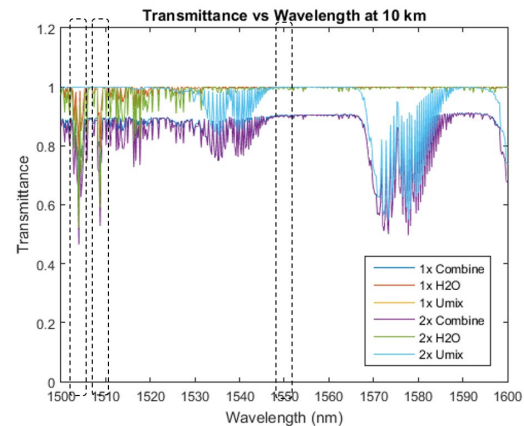

Figure 11. Combined, H2O, and Umix transmissivity is plotted at 10 km for 1.0 and 2.0 water vapor scaling factors. 1504 nm and 1509 nm show marked changes in transmissivity with water vapor scaling, while 1550 nm shows a near negligible change.

First we plot changes in combined, H2O, and uniformly mixed (Umix) transmissivity with both a 1.0 and 2.0 scaling factor as shown in Figure 11. We find that 1550 nm is a reasonable reference point because the combined transmissivity only varies 0.0002 between the 1.0 and 2.0 water vapor scaling factors. The 1504 and 1509 wavelengths show differences with water vapor scale factor changes that make them potential candidates for proximal wavelength pairing. At 1504 nm, the transmissivity changes from 0.69 to 0.47 when the water vapor scale factor doubles from 1.0 to 2.0. At 1508.8 nm, the

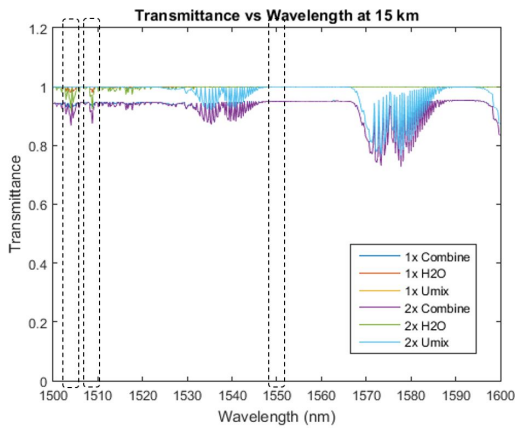transmissivity changes from 0.71 to 0.53 with a doubling of water vapor.

Figure 12. Transmissivity is plotted at 15 km for 1.0 and 2.0 water vapor scaling factors. 1504 nm and 1509 nm show a smaller change in transmissivity than at 10 km, but the change is still detectable.

Similarly, we plot the changes in transmissivity at 15 km for a 1.0 and 2.0 scaling factor of water vapor in Figure 12. The transmissivity shows smaller peaks at the same wavelengths as the 10 km analysis. In this case, the transmittance varies from 0.93 to 0.87 at 1504 nm, and from 0.93 to 0.87 at 1508.8 nm. Although this is a smaller decrease in transmittance, we assess that it should still be detectable for LCAS.
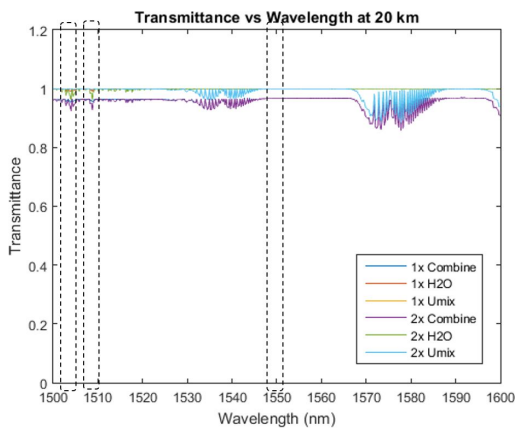

Figure 13. Transmissivity is plotted at 20 km for 1.0 and 2.0 water vapor scaling factors. At 20 km, the change in transmissivity at 1504 and 1509 nm has dropped to less than a 3% difference.

Next we plot the change in transmissivity with water vapor scaling at 20 km in Figure 13. At this altitude, the transmittance at 1504 and 1508.8 nm only drops from 0.96 to 0.93 with a doubling of water vapor. From this analysis, we expect that the optimal altitudes for LCAS between 1500 nm and 1600 nm will be from 10 km to 15 km; below 10 km may require additional transmit power to close a link.
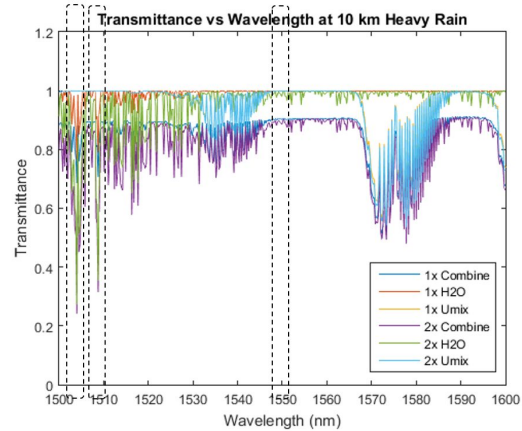

Figure 14. Transmissivity is plotted at 10 km for 1.0 and 2.0 water vapor scaling factors, but this time we include heavy rain and clouds in the simulation. Change in transmissivity is increased to a 45% difference with a doubling of water vapor.

We repeat the analysis at 10 km, but this time we add in heavy rain and clouds into the MODTRAN simulation to address concerns about experiment performance in the UTLS during weather events. The results are plotted in Figure 14. We show a higher percentage change at 10 km during heavy rain conditions than in clear sky, with a transmittance change from 0.69 to 0.24 at 1504 nm and a change from 0.71 to 0.31 at 1508.8 nm with a doubling in water vapor. Our reference frequency of 1550.4 nm remains stable. We summarize our results in Table 2.

To summarize the results in Table 1, we show the combined MODTRAN transmittance at three frequencies. 1550.4 nm shows a negligible change in transmittance with an increase in water vapor at all altitudes, and is chosen as our continuum frequency. 1504 nm and 1508.8 nm both show measurable differences in transmittances at 10 km and 15 km, and are satisfactory options to sound along the absorption features of water vapor.

Table 1: Change in Transmittance for Selected Wavelengths at 10, 15, and 20 km

Frequency (nm)	Combined Tx with H2O 1.0	Combined Tx with H2O 2.0	Differ-ence
Altitude: 10 km			
1504.0 nm	0.69	0.47	0.22
1508.8 nm	0.71	0.53	0.18
1550.4 nm	0.90	0.90	0.00
Altitude: 15 km			
1504.0 nm	0.93	0.87	0.06
1508.8 nm	0.93	0.87	0.06
1550.4 nm	0.95	0.95	0.00
Altitude: 20 km			
1504.0 nm	0.96	0.93	0.03
1508.8 nm	0.96	0.93	0.03
1550.4 nm	0.97	0.97	0.00
Altitude: 10 km (Heavy Rain)			
1504.0 nm	0.69	0.24	0.45
1508.8 nm	0.71	0.31	0.40
1550.4 nm	0.90	0.90	0.00

At 20 km, the change in transmittance may be too small; thus, we will aim for a tangent height from 10 km to 15 km for LCAS. The 10 km, 15 km, and 20 km analyses were completed for clear sky conditions. Our last analysis at 10 km simulated heavy rain and showed that LCAS would still be effective using 1550 nm, 1504 nm, and 1508.8 nm wavelengths during non-clear sky conditions.

Link Budget and Beamwidth Description

LCAS leverages architecture from the CubeSat Laser Infrared CrosslinK (CLICK) payload [22, 23, 24]. Table 1 provides an overview of the primary parameters included in CLICK's optical link analysis. For LCAS, unlike CLICK where a 20 Mbps data rate is required for the crosslink at 1537/1565 nm, there is no need for high rate throughput, so there is greater margin. Additional information on CLICK's beacon to camera and beacon to quadcell link analysis is included in the Appendix.

CLICK uses commercial-off-the-shelf (COTS) components to implement full-duplex laser communication. The receiver front-end consists of an Avalanche Photodiode (APD), RIP1-NJAF from Voxtel, Inc., as the baseline sensor, a Transimpedance Amplifier (TIA), integrated with the Voxtel APD, followed by a Bandpass Filter (BPF) and two Programmable Gain Amplifiers (PGAs). Two complementary architectures are implemented in the receiver: an Analog to Digital Converter (ADC) and Matched Filter (MF) and a comparator and Time to Digital Converter (TDC). The operation of these architectures is independent, to demonstrate different technologies, and selected by an electrical switch. In both cases, the signal is digitized, demodulated, and decoded by the receiver. Using Pulse Position Modulation (PPM), data rates exceeding 20 Mbps at Bit Error Rate (BER) of 10^{-4} can be achieved at a separation distance of hundreds of kilometers.

The average power limited Erbium Doped Fiber Amplifier (EDFA) for CLICK provides an output optical power of 200 mW for transmission, although higher power commercial EDFAs exist that may be able to be accommodated in a 6U or larger CubeSat. COTS opto-mechanical components are used to construct a telescope that focuses the transmit beam to a Full-Width Half-Max (FWHM) of 71 urad (0.004 degrees, 14.6 arcseconds). Unlike LCAS, atmospheric losses are negligible in the CLICK analysis, as the crosslink is assumed to take place in free space. The greatest loss contribution comes from the Free-Space Path Loss (FSPL) factor; proportional to the inverse of the range squared, high attenuation is expected at the given wavelength and separation ranges. The Voxtel APD has a high quantum efficiency resulting in a near-100% responsivity at 1550 nm (i.e. for each incident optical watt, one amp of electrical current is produced), and the received electrical power is directly proportional to received optical power. The dominant noise sources in the receiver are TIA thermal noise, the APD shot noise, and the APD dark current. The noise variances are Root Sum Squared (RSSed) to find the combined Power Spectral Density (PSD) and multiplied by the Noise Equivalent Bandwidth (NEB) of the TIA to determine the total power of the noise present in the receiver. A threshold of 3dB margin is kept between the power received and power required. The beacon to camera and beacon to quadcell analyses are included as supplementary information in the appendix. The ACCURATE study includes detailed link budgets and atmospheric absorption analyses for wavelengths further in the near infrared than CLICK [6].

It is necessary to adapt the CLICK link analysis to incorporate additional parameters such as target

species absorption loss, background loss for the absorption channel, as well as anticipated errors in the reference or absorption channels, species absorption coefficient and absorption cross section. The required inter-satellite crosslink range for an occultation event will be much larger for LCAS, with ~5100 km of separation between two occulting LEO satellites. Changes to the CLICK architecture to increase the transmit beacon power, increase the receiver aperture, or decrease the beacon divergence are examples of some of the many feasible options under consideration.

Future analysis is necessary to expand the wavelength space from 1500 nm to 1600 nm to assess absorption and continuum features using MODTRAN, as well as a refinement to the atmospheric modeling approach beyond the simple increase in water vapor factor. More detailed analyses modeling target absorption features and their expected attenuation levels at incremental tangent heights to extract more precise parameters for the link analysis are planned. In addition, a reassessment of the minimum data rate necessary to close an occultation crosslink (as opposed to a communications link) investigation of alternate modulation schemes for maximizing range between the two occulting LEO spacecraft are planned.

Additionally, we plan to refine the optical link analysis with more precise estimates of expected losses and errors. Numerical simulations of parameters such as background loss for the absorption channel will help to improve the accuracy of these estimates.

FUTURE WORK

The CLICK PPM transceiver which could be used for LCAS is currently in development, and to be fabricated and tested in a package consistent with the CubeSat form factor. The seed laser has been developed as a part of the NODE payload [27] and needs to be integrated into the transceiver. The APD receiver and its amplification chain have been prototyped and demonstrated, its performance is suitable for CLICK, although it may require improvements to meet the requirements of LCAS.

The CLICK pointing, acquisition, and tracking system will need be verified with robustness to atmospheric disturbances. This can be done by modifying the CLICK hardware in the loop testbeds to verify the system's ability to support a 120 urad

beamwidth. Optomechanical assembly procedures and calibration will also require updates to ensure the pointing budget closes. The onboard pointing equivalent angle estimator for the quadcell will be adapted from the CLICK software.

Table 2: Overview of key parameters in the CLICK inter-satellite link analysis.The link analysis is completed for 20 Mbps data rate and 1537/1565 nm wavelengths.

Inter-Satellite Crosslink Budget	
Range (km)	855.00
PPM Order	16.00
Transmit Power (dBW)	-6.99
Full Width Half Maximum (mrad)	0.07
Beam Solid Angle (steradians)	3.96E-09
Transmitter Gain (dBi)	95.02
Transmitter Loss (dB)	-1.74
Receiver Gain (dBi)	92.16
Receiver Loss (dB)	-1.75
Path Loss (dB)	-257.54
Atmospheric Loss (dB)	0.00
Pointing Loss (dB)	-3.00
Power Received (dBW)	-83.36
Power Required (dBW)	-86.44
Margin	**2.98**

The relative pointing estimator used to close the loop on satellite tracking will need improved robustness properties for stale relative orbit data and atmospheric disturbances to the beacon camera receive signal. The acquisition procedure will need to be improved with search algorithms designed to accommodate reduced orbit knowledge as beamwidth.

We have baselined the the CLICK 500 km, 80 degrees inclination circular orbit for our analysis, with the second spacecraft in a 100 degree inclination counter-rotating orbit in the same orbital plane. The number of occultation opportunities and occultation distance have been calculated based on the CLICK baseline orbit. Future work will analyze the optimal orbit selection for the LCAS spacecraft (i.e. altitude,

inclination, and phasing) in order to maximize occultation opportunities that can be achieved with each pass, and we will update our estimates of number and distance of occultations based on the updated orbit selected.

The MODTRAN analysis will continue to be improved in order to refine the estimates of transmissivity with water vapor concentration. Instead of assuming 1.0, 2.0, and 3.0 scale factors of water vapor, we will provide more refined estimates of water vapor concentrations in parts per million per volume (ppmv). We chose initial analyses at 10 km, 15 km, and 20 km; we will refine the analyses and determine the optimal tangent heights to be used for the LCAS lasercom crosslinks.

Future work will also be completed in order to update the CLICK crosslink budget for LCAS. We will update parameters such as range, PPM order, wavelength, and atmospheric losses and determine data rate that can be achieved for the crosslink. We will additionally analyze hardware updates to the CLICK architecture that could be implemented in order to increase power, increase aperture size, and/or decrease beacon FWHM in order to optimize crosslink range.

CONCLUSION

LCAS proposes a novel method of using only laser crosslinks to obtain both bending angle (temperature profile) and composition information for atmospheric sounding. The two occulting LEO CubeSats assessed in this work are placed in counter-rotating 500 km orbits with 80 degree and 100 degree inclinations, enabling them to retrieve 31 along-track occultation measurements per day. Other occultation geometries in LEO can also be supported, and a full trade study is planned to maximize number of along-track occultation measurements per day.

MODTRAN analyses determine that wavelengths of 1550 nm, 1504 nm, and 1508.8 nm to be sufficient for recovering water vapor and temperature measurements within the UTLS with high vertical resolution during non-clear sky conditions. Future analyses will both extend the wavelength range going beyond a demonstration mission with a couple of wavelengths toward an operational mission with many. Also, analyses that assess the precision with which this approach can obtain concurrent temperature profiles and composition will be performed.

Based on architecture used in the CLICK demonstration, the crosslink analysis shows that a transmit beacon beam with a half power beamwidth of 0.01 rad (see Table A.4) and 10 dBW output power is sufficient for closing the link at 5000 km separation between spacecraft. The ACCURATE study demonstrates also a successful transmit link with output power on the order of 1W [6]. Future link analysis will be performed to refine the transmit power and modulation type.

GPSRO systems are approximately the same targeted size, weight, and power as LCAS, but cannot retrieve water vapor abundance although they are affected by it. LCAS demonstrates the novel approach of a laser occultation system using wavelength-stabilized and calibrated, paired, full-duplex crosslink beams, to concurrently recover both composition and temperature with high accuracy and high vertical resolution. This method has the potential to improve the vertical resolution of temperature profiles compared to GPS RO techniques.

Supplementing preexisting atmospheric information with high resolution data would offer further insight on the atmosphere's molecular composition, including aerosols, and, over extended periods of time, its response to changes in climate. Demonstration of the LCAS system concept and follow-on operational implementation would improve data for weather and climate models. For example, this measurement can address ozone depletion following convective injection of water vapor into the UTLS and other issues related to stratospheric humidification.

BIBLIOGRAPHY

[1] J. Anderson, D. Weisenstein, K. Bowman, et al., "Stratospheric ozone over the united states in summer linked to observations of convection and temperature via chlorine and bromine catalysis," PNAS Early Edition (2017).

[2] E. R. Kursinski, G. A. Hajj, J. T. Schofield, et al., "Observing Earth's atmosphere with radio occultation measurements using the Global Positioning System," *J. Geophys. Res.*, 102(D19), 23429–23465 (1997).

[3] S. Schweitzer, G. Kirchengast, and V. Proschek, "Atmospheric influences on infrared-laser signals used for occultation measurements between low earth

orbit satellites," Geophysical Research Letters 38 (2011).

[4] U. Sterr, D. Dallman, F. Heine, et al., "Planning constraints of low grazing altitude geo-leo laser links based on in-orbit data," Optical Engineering 55 (2016).

[5] J. Harrison, P. Bernath, and G. Kirchengast, "Spectroscopic requirements for accurate, a microwave and infrared laser occultation satellite mission," Journal of Quantitative Spectroscopy and Radiative Transfer 112 (2011).

[6] Kirchengast and Scheweitzer, "ACCURATE LEO-LEO Infrared Laser Occultation Initial Assessment: Requirements, Payload Characteristics, Scientific Performance Analysis, and Breadboarding Specifications," WegCenter/UniGraz Technical Report (2007).

[7] J. Conklin, N. Barnwell, L. Caro, et al., "Optical time transfer for future disaggregated small satellite navigation systems," (2014).

[8] H. Yoon, *Pointing System Performance Analysis for Optical Inter-satellite Communication on CubeSats*. PhD thesis, Massachusetts Institute of Technology (2017).

[9] J. Waters, L. Froidevaux, R. Harwood, et al., "The earth observing system microwave limb sounder (eos mls) on the aura satellite," IEEE Transactions on Geoscience and Remote Sensing 44 (2006).

[10] "Ohio state university astronomy department." http://www.astronomy.
ohio-state.edu/pogge/Ast161/Unit5/atmos.html.

[11] "Gemini telescope." http://www.gemini.edu/sciops/telescopes-and-sites/observing-condition-constraints/ir-transmission-spectra.

[12] "Itu bands." http://a2net.eu/fiberoptics.html.

[13] A. D. Marinan, *Improving Nanosatellite Capabilities for Atmospheric Sounding and Characterization*. PhD thesis, Massachusetts Institute of Technology (2016).

[14] G. Kirchengast and S. Schweitzer, "Climate benchmark profiling of greenhouse gases and

thermodynamic structure and wind from space," Geophysical Research Letters 38 (2011).

[15] G. Kirchengast and S. Schweitzer, "Auxiliary material for paper 2011gl047617 climate benchmark profiling of greenhouse gases and thermodynamic structure and wind from space," Geophysical Research Letters (2011).

[16] "CHAMP profile from eumetsat." http://www.eumetsat.int/eps_webcast/eps/print.htm#s8p3.

[17] G. Hajj, E. Kursinski, L. Romans, et al., "A technical description of atmospheric sounding by gps occultation," Journal of Atmospheric and Solar-Terrestrial Physics 64 (2002).

[18] E. Kursinski, D. Ward, A. Otarola, et al., "The Active Temperature, Ozone and Moisture Microwave Spectrometer (ATOMMS)," New Horizons in Occultation Research (2009).

[19] J. Conklin, N. Barnwell, L. Caro, et al., "Optical time transfer for future disaggregated small satellite navigation systems," (2014).

[20] H. Yoon, K. Riesing, and K. Cahoy, "Kalman filtering for attitude and parameter estimation of nanosatellites without gyroscopes," Journal of Guidance, Control, and Dynamics (2017).

[21] E. Miller, K. Birnbaum, C. Chen, A. Grier, M. Hunwardsen, and D. Jandrain, "Fine Pointing and Tracking Concepts for Optical Intersatellite Links," no. Cdm, pp. 218–223, 2017.

[22] P. Grenfell, A. Aguilar, K. Cahoy, "Pointing, Acquisition, and Tracking for Small Satellite Laser Communications," *Proceedings of the AIAA/USU Conference on Small Satellites, Advanced Concepts I, SSC18-WKI-01,* (2018).

[23] M. Long, "Pointing Acquisition and Tracking Design And Analysis for CubeSat Laser Communication Crosslinks," Masters thesis, Massachusetts Institute of Technology (2018).

[24] A. Crews, "CubeSat Laser Infrared CrosslinK (CLICK)," *CubeSat Developers Workshop* (2018).

[25] R. W. Kingsbury, "Optical Communications for Small Satellites," PhD thesis, Massachusetts Institute of Technology (2015)

[26] Klaus Abich et al, "GRACE-Follow On Laser Ranging Interferometer: German contribution," *Journal of Physics: Conference Series*, vol. 610, no. 1, p. 012010, 2015.

[27] Clements, Emily et al. "Nanosatellite Optical Downlink Experiment: Design, Simulation, and Prototyping." Optical Engineering 55.11 (2016): 111610.

APPENDIX I

Beacon to Camera

The beacon to camera link is the second stage in CLICK's Position, Acquisition and Tracking (PAT) sequence. Each satellite powers on a beacon transmitter and a Wide Field Of View (WFOV) sensor (camera); then, each satellite transmits a beacon signal at 976 nm and receives the opposing satellite's signal on the respective sensors. Once a spacecraft has acquired a beacon signal, closed-loop feedback control is established with the reaction wheels to maintain Line Of Sight (LOS) with coarse body pointing. The beacon divergence angle and WFOV sensor have been designed such that no search pattern is required; this is an acquisition method for risk mitigation known as "stare-stare."

Beacon to Quadcell

The beacon to quadcell link is the third stage in CLICK's PAT sequence. After coarse pointing control
has been established, the beacon signal is directed down a beam reducer, reflected off of a Fast Steering Mirror (FSM), and focused onto a photodetector known as a quadcell. A closed feedback loop for fine pointing control is formed between the FSM and the quadcell; as the beacon signal drifts on the detector, the FSM is actuated to center the received signal. This enables fine pointing capability for the transmitter beam used in the laser crosslink, and allows the received laser communication signal to be steered within the field of view (FOV) of the APD.

Table A.1. CLICK Beacon to Camera Budget

Link Range (km)	5	100	500	850	1000	1500
Beacon Optical Power (dBW)	-3.01	-3.01	-3.01	-3.01	-3.01	-3.01
Beacon Wavelength (m)	9.76E-07	9.76E-07	9.76E-07	9.76E-07	9.76E-07	9.76E-07
Pointing Loss (dB)	-3.00	-3.00	-3.00	-3.00	-3.00	-3.00
Half Power Beamwidth (rad)	0.01	0.01	0.01	0.01	0.01	0.01
FSO Path Loss (dB)	-216.17	-242.20	-256.17	-260.78	-262.20	-265.72
Tx Optics Loss (dB)	-0.40	-0.40	-0.40	-0.40	-0.40	-0.40
Rx Optics Loss (dB)	-0.10	-0.10	-0.10	-0.10	-0.10	-0.10
Receiver Aperture Diameter (mm)	20.00	20.00	20.00	20.00	20.00	20.00
Sensor Quantum Efficiency	0.02	0.02	0.02	0.02	0.02	0.02
SNR	31.97	18.94	11.55	8.62	7.62	4.88

Table A.2 LCAS Beacon to Camera Budget

Link Range (km)	5	1000	2000	5000	6000	7000
Beacon Optical Power (dBW)	10.00	10.00	10.00	10.00	10.00	10.00
Beacon Wavelength (m)	9.76E-07	9.76E-07	9.76E-07	9.76E-07	9.76E-07	9.76E-07
Pointing Loss (dB)	-3.00	-3.00	-3.00	-3.00	-3.00	-3.00
Half Power Beamwidth (rad)	0.01	0.01	0.01	0.01	0.01	0.01
FSO Path Loss (dB)	-216.17	-262.20	-268.22	-276.17	-277.76	-279.10
Tx Optics Loss (dB)	-0.40	-0.40	-0.40	-0.40	-0.40	-0.40
Rx Optics Loss (dB)	-0.10	-0.10	-0.10	-0.10	-0.10	-0.10
Receiver Aperture Diameter (mm)	20.00	20.00	20.00	20.00	20.00	20.00
Sensor Quantum Efficiency	0.02	0.02	0.02	0.02	0.02	0.02
SNR	31.97	15.37	12.11	6.9	5.67	4.57

Table A.3. CLICK Beacon to Quadcell Link Budget

Link Range (km)	100	500	850	1000
Beacon Optical Power (dBW)	-3.01	-3.01	-3.01	-3.01
Beacon Wavelength (m)	9.76E-07	9.76E-07	9.76E-07	9.76E-07
Pointing Loss (dB)	-0.50	-0.50	-0.50	-0.50
Half Power Beamwidth (rad)	0.01	0.01	0.01	0.01
FSO Path Loss (dB)	-242.20	-256.17	-260.78	-262.20
Tx Optics Loss (dB)	-0.40	-0.40	-0.40	-0.40
Rx Optics Loss (dB)	-0.32	-0.32	-0.32	-0.32
Receiver Aperture Diameter (mm)	20.00	20.00	20.00	20.00
Sensor Responsivity (A/W)	0.62	0.62	0.62	0.62
SNR (dB)	26.52	18.76	15.46	14.33

Table A.4. LCAS Beacon to Quadcell Link Budget

Link Range (km)	1000	2000	5000	5800
Beacon Optical Power (dBW)	10	10	10	10
Beacon Wavelength (m)	9.76E-07	9.76E-07	9.76E-07	9.76E-07
Pointing Loss (dB)	-0.50	-0.50	-0.50	-0.50
Half Power Beamwidth (rad)	0.01	0.01	0.01	0.01
FSO Path Loss (dB)	-262.20	-268.22	-276.17	-277.46
Tx Optics Loss (dB)	-0.40	-0.40	-0.40	-0.40
Rx Optics Loss (dB)	-0.32	-0.32	-0.32	-0.32
Receiver Aperture Diameter (mm)	30.00	30.00	30.00	30.00
Sensor Responsivity (A/W)	0.62	0.62	0.62	0.62
SNR (dB)	24.71	21.43	16.08	15.05

Table A.5. CLICK Acquisition Pointing Budget [23]

Error Source	Allocated	Expected
Sat A Orbit Estimation	345	295
Sat B Orbit Estimation	775	726
ADCS Precision	43	32
Residual Calibration Error	315	252
Launch Induced Shift	40	30
Thermal Deformation	295	234
Acquisition Error	954	857
Margin	10%	
*Values are Single-Axis Half-Angles (3 σ), units: arcsec		

Table A.6. CLICK CPS Field Angle Estimation [8,23]

Error Source	Estimate
CPS Residual Pointing Error (Simulated)	42
Residual Calibration Error	20
Launch Induced Shift	2
Thermal Deformation	1
Launch Induced Shift	40
CPS Field Angle Estimate	61
*Values are Single-Axis Half-Angles (3 σ), units: arcsec	

Table A.7. CLICK Fine Pointing Budget [8,23]

Error Source	Allocated	Expected
FSM 1	0.2	0.1
Quadcell	2.4	2.21
Spaceraft Jitter	0.2	0.1
Optical Misalignments	4.6	4.5
Chromatic Field Error	0.15	0.1
Fine Pointing Error	5.2	5.0
Margin	3.5%	
*Values are Single-Axis Half-Angles (3σ), units: arcsec		